Article

Efficient Removal of Azlocillin Sodium from Water by Polystyrene Anion Exchange Resin Supported MIL-53

Yi Qian [1,*], Haoyan Fu [1], Long Li [2,*], Wenyuan Su [1], Jiayin Li [2] and Yihao Zhang [2]

1   College of Chemical Engineering, Qingdao University of Science and Technology, Qingdao 266042, China; fuhaoyanfhy@163.com (H.F.); suwenyuan1226@163.com (W.S.)
2   College of Environment and Safety Engineering, Qingdao University of Science and Technology, Qingdao 266042, China; lijiayin085@163.com (J.L.); 18832623721@163.com (Y.Z.)
*   Correspondence: qianyi@qust.edu.cn (Y.Q.); lli@yic.ac.cn (L.L.)

Academic Editor: Avelino Núñez-Delgado

Publisher's Note: MDPI stays neutral with regard to jurisdictional claims in published maps and institutional affiliations.

Abstract: Due to the widespread use of antibiotics in medical treatment, animal husbandry and aquaculture, a large number of antibiotics are discharged into the environment as metabolites or in their original state, causing pollution to water bodies, which is a serious issue. In this study, a novel nanocomposite adsorbent MIL-53/D201 was successfully prepared by hydrothermal synthesis. This approach overcomes the disadvantage of easy dissociation of MOF material in the water phase and realizes the efficient removal of antibiotic azlocillin sodium in water. The crystal morphology and basic structure of the composites were characterized by X-ray diffraction (XRD), Fourier transform infrared spectroscopy (FTIR), scanning electron microscopy (SEM), energy scattering spectroscopy (EDS), and specific surface area and porosity analyzer (BET). The results showed that MIL-53 was successfully synthesized in situ in D201. The results of adsorption experiments show that the maximum saturated adsorption capacity of the composite is 122.3 mg/g when the dosage of the composite is 1.0 g/L. Compared with pure MIL-53 material, the composite material exhibits greater stability and efficient adsorption performance for target pollutants at different pH values. The adsorption process accords with the quasi-second-order kinetic adsorption model and Langmuir adsorption isothermal model. After five cycles of adsorption and desorption, the removal rate of MIL-53/D201 to azlocillin sodium was still above 87%.

Keywords: MOF; polystyrene macroporous resin; adsorption; antibiotics; in situ synthesis

1. Introduction

As a result of the aggravation of water pollution and the upgrade in the national environmental protection strategy, research into purification methods for water pollutants has become a popular topic in the environmental field [1]. Antibiotics are also commonly used in aquaculture because of intensive farming. Compared with other pollutants, antibiotics have higher bioavailability and longer environmental retention time, and can thus pose a significant threat to the aquatic ecosystem at the PPM and ppb levels. As a result, these issues have attracted extensive attention in recent years [2–5]. As an oxygen-containing anion antibiotic, azlocillin sodium is widely used in various infections caused by Gram-positive and -negative bacteria and Pseudomonas aeruginosa infection. Its uses include treatment of sepsis, meningitis, the gastrointestinal tract, the bile duct, the urinary tract, reproductive organs, skin burns, and other diseases, and it cannot be effectively removed by biodegradation. When azlocillin sodium enters the human body, 30% to 90% of its active ingredients are excreted without changing their properties. These substances may directly or indirectly enter the water system environment, thus causing pollution. In addition, the massive influx of antibiotics into water bodies has led to an increase in antibiotic-resistant bacteria, known as "antibiotic resistance pollution" [6]. At present, many treatment processes have been proposed to solve these problems, such as chemical precipitation, flocculation, advanced oxidation, and membrane filtration. However, these

methods have a high cost, readily produce secondary pollution, and cannot easily remove pollutants to acceptable concentrations. These challenges limit their practical application. For example, membrane separation is not suitable for large-scale applications because of its short lifetime, limited performance at low pressure, and poor stability in acid gas environments [7]. Compared with the above methods, adsorption technology is favored by scientific research and engineering fields because of its advantages of lower cost, easy design, and regeneration [1,8]. Unfortunately, improvement is required in traditional adsorption materials such as zeolite, activated carbon, and hydrotalcite in terms of adsorption capacity and adsorption selectivity [9–11], and the development of new efficient adsorbent materials for water pollutants remains an urgent unresolved problem.

The metal-organic framework (MOF) is a new kind of nano-adsorption material, which is a porous crystal material formed by metal ion clusters and organic ligands through coordination links. The transition metal ions provide the catalytic center for MOF, and the organic ligands provide the functional branch chain structure [12]. Therefore, MOF material is more abundant in structural changes and has significant advantages in adsorption capacity and selectivity compared with other adsorbents [13,14]. In addition, MOF is one of the most promising adsorbents, having the advantages of large specific surface area, channel tunability, and small particle size for rapid water filtration [15–17]. For example, Lee and colleagues previously developed a series of robust MOFs with a 3D framework and high surface area volume ratio, showing excellent antibacterial activity against *Escherichia coli* and *Staphylococcus aureus*. This is highly relevant to the current work [18,19]. Ma and coworkers synthesized three iron-based MOFs for adsorption of a typical volatile organic compound, toluene [20]. However, the particle size of MOF material is mostly at the micron level, and it is difficult to separate from the water phase after adsorption. Therefore, when used as the filler of a rapid filtration device, the pressure drop is large; thus, the hydrodynamic performance is poor. Secondly, due to the size of the organic ligand, most MOF materials are microporous, and the diffusion rate of the adsorbent is slow during the adsorption process, resulting in poor adsorption kinetic performance [21–23]. Thirdly, the structural integrity of MOF material depends on the coordination between organic ligands and metal ion clusters, and it is easily dissociated in the water phase [24–26]. MIL-53 is a three-dimensional porous solid linked by numerous -Fe-O-O-Fe-O-Fe- bonds and crosslinked by terephthalate. Its chemical structure is shown in Figure 1, and it has the advantages of low cost and non-toxicity. MIL-53 also shows considerable adsorption and photocatalytic activity in wastewater treatment, which makes it a potential candidate material for environmental remediation [27,28]. However, MIL-53 is extremely unstable in an aqueous solution. It is a challenge to achieve optimal performance of MIL-53 by directly suspending it in water as an adsorbent to remove organic pollutants [29]. To overcome the above shortcomings of MOF, there is an urgent need to find a stable polymer material as a carrier, and fix MOF onto this carrier to prepare more stable and efficient composite adsorption materials. Polystyrene macroporous resin (for example, D201 resin is an anion exchange resin) has high mechanical and chemical stability and excellent hydrodynamics performance. The covalently linked quaternary ammonium groups on the polystyrene framework can preconcentrate the target ions through ion exchange [30]. By loading inorganic adsorption materials into macroporous resins, a variety of efficient composite adsorption materials can be developed [31–33]. However, little research has been done on impregnating MOF into macroporous anion exchange resins to remove contaminants from water.

In summary, in this study, MIL-53 material was in situ synthesized in D201 macroporous resin to prepare MIL-53/D201 composite material, for use in the adsorption of azlocillin sodium in water. The preparation method of the composite was systematically studied by investigating the microstructure, surface properties, and internal structure of the composite. Based on the properties of pores, specific surface area, and ion exchange capacity, the experimental conditions were optimized to prepare the composite with good properties. The composite material was used for the adsorption of azlocillin sodium, and

the effects of adsorption time, adsorbent dosage, solution PH, and different interfering ions on the adsorption performance of MIL-53/D201 composite were studied. The adsorption performance was investigated by batch adsorption experiments, the relevant thermodynamic parameters were obtained, and the adsorption mechanism was explored.
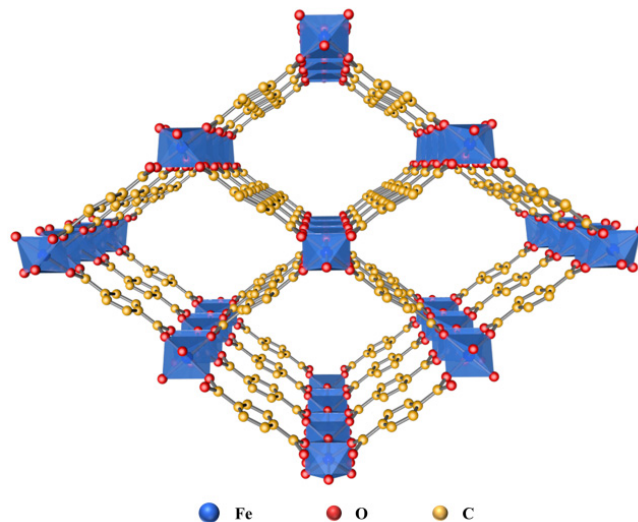

Figure 1. The schematic 3D representation of MIL-53.

2. Materials and Methods

2.1. Materials

Ferric chloride hexahydrate ($FeCl_3 \cdot 6H_2O$, 99%), N, N-dimethylformamide (DMF, 99%), terephthalic acid (H_2BDC, 99%), and ethanol (C_2H_5OH) was purchased from Shanghai Maclin Biochemical Technology Co., LTD (Shanghai, China). Sodium hydroxide (NaOH) and nitric acid (HNO_3) were purchased from Shanghai Aladdin Chemical Reagent Co., LTD. Azlocillin sodium was purchased from Sinopharm Chemical Reagent Co., LTD (Shanghai, China). These reagents were analytical grade and used without further purification. D201 macroporous resin was purchased from Zhengzhou Kelisen Chemical Technology Co., LTD (Zhengzhou China). Ultra-pure water was used in all experiments.

2.2. Preparation of MIL-53/D201 Composite

MIl-53/D201 composite was prepared by the hydrothermal synthesis method (Figure 2). D201 was extracted with acetone in a Soxhlet apparatus to remove possible residual impurities and dried in an oven at 60 °C for later use. First, ferric chloride hexahydrate (5 mmol) and D201 macroporous resin (0.5 g) were dissolved in N, N-dimethylformamide solution (30 mL) and stirred at room temperature for 1 h, denoted as solution 1. Then, terephthalic acid (5 mmol) was dissolved in N, N-dimethylformamide solution (30 mL), and ultrasound was performed for 20 min, denoted as solution 2. Solution 1 and solution 2 were quickly mixed, fully stirred at room temperature for 2 h, then transferred to a 100 mL Teflon reactor and heated at 150° for 15 h. After the reactor was cooled to room temperature, the product was centrifuged and washed several times with N, N-dimethylformamide, and finally placed in a 60° vacuum drying oven overnight to obtain MIL-53/D201 composite.

2.3. Characterizations

X-ray diffraction (XRD) testing was performed with a Rigaku X-ray Diffractometer (Shimadzu Corporation of Japan, Tokyo, Japan), which uses Cu-Kα tubes and Ni filters (λ = 0.1542 nm). Fourier transform infrared spectroscopy (FTIR) in the wavelength range of 500–4000 cm^{-1} was recorded on a Nicolet-6700 FTIR spectrometer (PerkinElmer, Waltham, MA, USA). The JMS-6700 scanning electron microscope (SEM) and energy spectrum (EDS) were used to analyze and test the samples. The tested sample was sprayed with gold five times, and the acceleration voltage was 10 kV. The N_2 adsorption-desorption process of the

composite was tested at 77 K by ASAP2020 specific surface area and porosity analyzer (BET), and N_2 adsorption and desorption isotherms and pore size distribution were obtained.
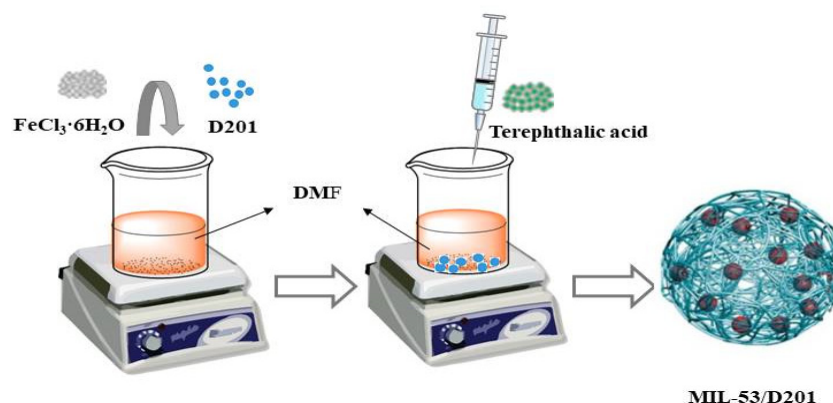

Figure 2. Schematic illustration of preparation process of MIL-53/D201 composite material.

2.4. Adsorption Experiment and Regeneration Experiment

In order to study the mass ratio with high adsorption performance, a certain amount of MIl-53/D201 composite material was placed in a 250 mL conical flask, and 200 mL sodium azlocillin solution (1 mmol/L) was added at the same time and adsorbed by a water bath shaker under constant temperature (25 °C). The solution pH was adjusted with 0.1 mol/L nitric acid (analytically pure) and 0.1 mol/L sodium hydroxide (analytically pure), and the adsorption of MIL-53 and MIL-53/D201 composite in the pH range (1.0 to 11.0) was investigated. Considering that the actual wastewater treatment is more complicated, Cl^-, SO_4^{2-}, and SiO_3^{2-} were selected as interference ions. The adsorption experiments were carried out by adding 100 mg MIL-53/D201 composite material to 200 mL of azlocillin sodium solution with different concentrations of three interfering ions. In order to determine the recoverability of MIL-53/D201 composite adsorbent, the adsorbent after adsorption balance was washed with deionized water and soaked in ethanol solution at room temperature for 24 h for desorption, so as to completely eliminate the adsorbed azlocillin sodium. The regenerated MIL-53/D201 composite was used in the adsorption experiment again, and the cycle was repeated five times. All of the above adsorption and regeneration experiments were carried out at room temperature (25 °C) with a water bath shaker at a speed of 350 RPM. The solution was centrifuged in a conical flask. The supernatant was extracted using an injection filter (hydrophobic, 0.5 µm) and the concentration of the remaining azlocillin sodium solution was analyzed by UV spectrum. The adsorption capacity and efficiency of the adsorbent can be calculated by the following equations:

$$q_e = \frac{(C_0 - C_e)V}{m},$$ (1)

$$E(\%) = \frac{C_0 - C_e}{C_0} \times 100\%,$$ (2)

where C_0 and C_e (g/mL) were the initial and equilibrium concentrations of azlocillin sodium, respectively. q_e represents adsorption capacity (mg/g); V represents the volume of solution (mL); and M represents adsorbent mass (g).

3. Results and Discussions

3.1. Characterization

XRD is usually used to characterize the crystal structure of materials. Figure 3a shows X-ray diffraction patterns of D201, MIL-53, and MIL-53/D201 composite. It can be seen from the figure that although D201 has no obvious characteristic peak, it has characteristic fluctuation in the range 2θ = 15–25. The crystal structure of MIL-53 has sharp and clear characteristic peaks at 2θ = 9.3, 12.6, 16.8, 17.9, 25.5, 27.32, 29.8, 30.28, and 36.18. This

indicates that the prepared MIL-53 material has a good crystal structure, which is consistent with the results reported in the literature [34]. In addition, in the XRD patterns of MIL-53/D201 composite, we can see that the material at 2θ = 9.3, 12.6, 16.8, 17.9 and 25.5 has the characteristic peaks of MIL-53 and the characteristic fluctuations of D201. The results showed that MIL-53/D201 composite was successfully synthesized.
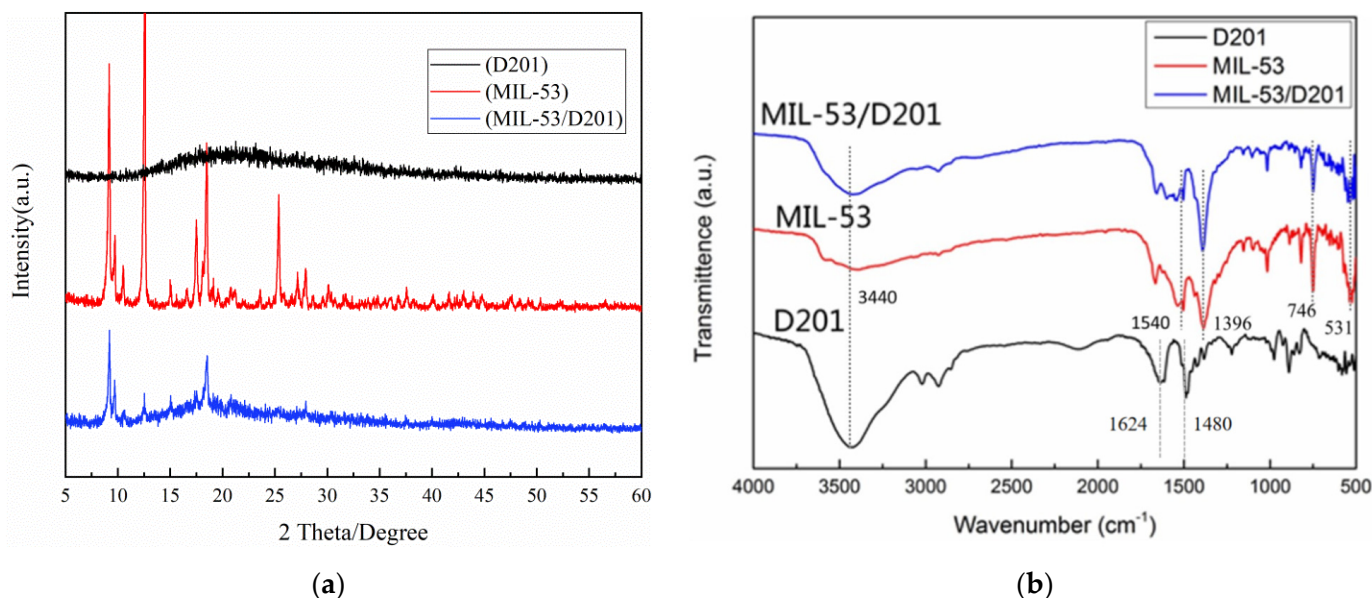

(**a**) (**b**)

Figure 3. XRD (**a**) and FT−IR (**b**) of MIL-53/D201 composite and their components.

FTIR study further confirmed the successful synthesis of MIL-53/D201 composite (Figure 3b). These results showed that the infrared absorption spectra of MIL-53 are highly consistent with the data reported in the literature [35]. The peaks at 746 and 533 cm^{-1} correspond to the vibration of the C-H bond in the benzene ring and the formation of the metal-oxygen bond between the carboxyl group of terephthalic acid and Fe^{3+}, respectively. The region between 1300 and 1700 cm^{-1} is associated with carboxylic acid ligands, indicating the coordination of H$_2$BDC with iron centers. The two peaks of MIL-53 at 1540 and 1380 cm^{-1} correspond to the asymmetric vibration of the carboxyl group and the symmetric vibration of the carboxyl group, respectively, which proves the existence of dicarboxylic acid bonds in the sample. The wide peak centered at 3440 cm^{-1} is related to the stretching vibration of the water-adsorbed O-H. The characteristic peaks of D201 macroporous resin at 1624 and 1480 cm^{-1} are mainly related to the -N$^+$(CH$_3$)$_3$ group.

By comparing the FTIR spectra of the MIL-53/D201 composite, it was found that the stretching vibration of the characteristic bond of MIL-53 and D201 anion exchange resin was shown in the FTIR spectra of MIL-53/D201 composite, which further demonstrated the successful preparation of the composite adsorption material.

As shown in Figure 4, the morphology of MIL-53, D201 macroporous resin, and MIL-53/D201 composite material was analyzed by SEM. MIL-53 was observed to have an irregular blocky structure (Figure 4a) dominated by a rod-like structure with smooth surfaces and straight edges (Figure 4b), which is consistent with previously reported results [36]. The parent anion exchange resin bead has a smooth surface and is free of any particles (Figure 4c) [37]. There are many dense pores in the D201 macroporous resin (Figure 4d). Figure 4e,f show SEM images of the surface and cross section of MIL-53/D201 composite material, respectively. It can be seen that MIL-53 is evenly dispersed on the surface of D201 resin. MIL-53 still maintains a clear rod-like structure inside the resin and has close interface contact with the resin.
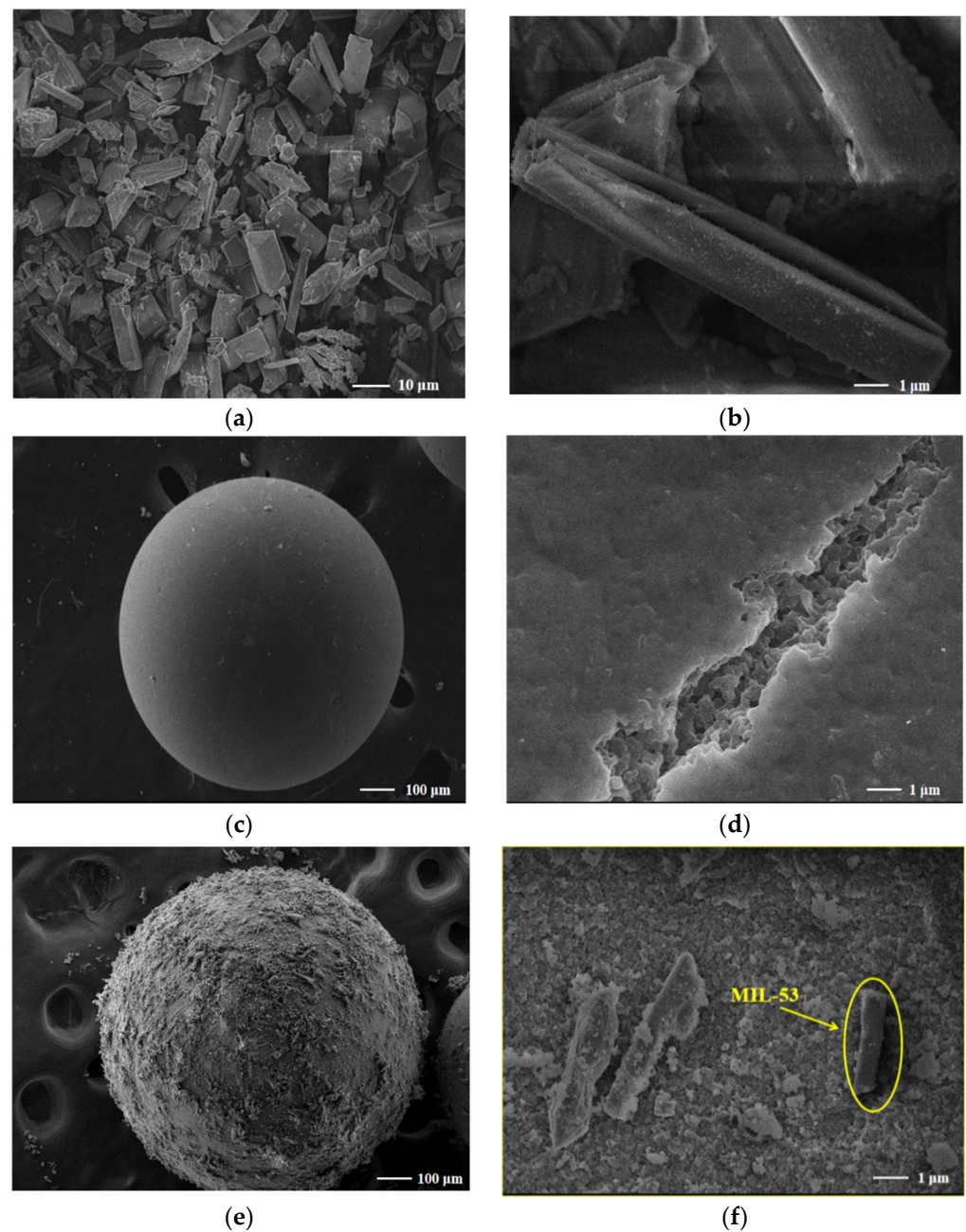
Figure 4. SEM image of MIL-53 (**a**,**b**), D201 (**c**,**d**), MIL-53/D201 composite (**e**), and MIL-53/D201 composite transverse section (**f**) at different magnifications.

Figure 5 shows the element distribution diagram and energy spectrum analysis diagram of MIL-53/D201 composite in cross section. Figure 5a,b of the element distribution in the cross section shows that Fe and Cl are not only distributed on the outside of the resin, but also on the inside of the resin, indicating that MIL-53 was successfully synthesized in situ inside the resin. Figure 5c clearly shows that the main components of MIL-53/D201 composite are C, O, N, Fe, and Cl. The presence of Cl in the material sample of MIL-53/D201 composite is due to the random absence of organic ligands in the entire material frame, resulting in charge and coordination defects, which can be compensated for by Cl^{-}.
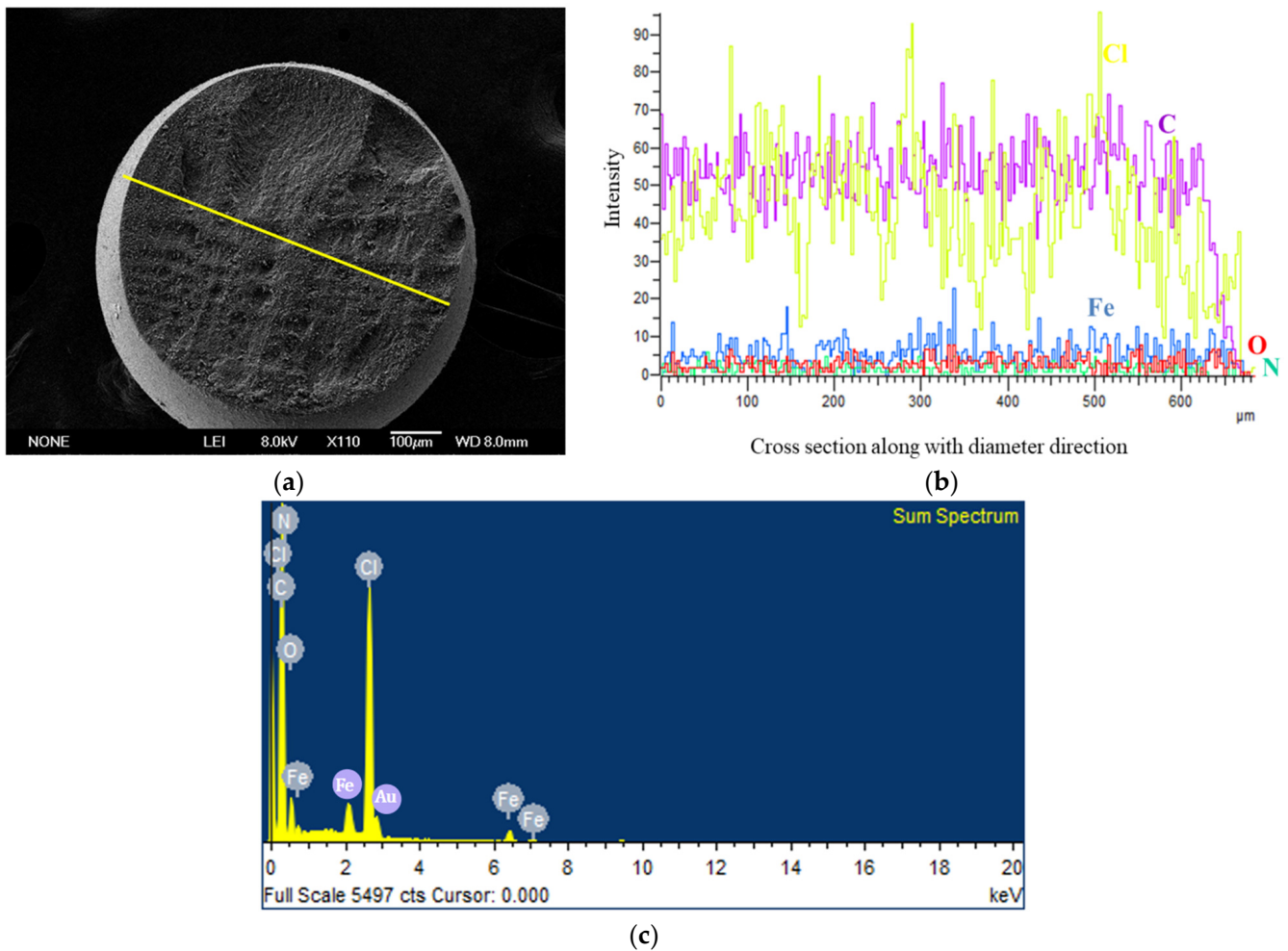
Figure 5. Cross section SEM image (**a**), element distribution diagram (**b**), and EDS spectrum analysis diagram (**c**) of MIL-53/D201.

Based on BET test analysis of MIL-53/D201 composite anion-exchange resin composite, N_2 adsorption and desorption isotherms (Figure 6a) and BJH pore size distribution (Figure 6b) were obtained. The total specific surface area of composites was calculated by the BET equation. The BET equation is as follows:

$$\frac{P}{V\,(P_0 - P)} = \frac{1}{V_M C} + \frac{C - 1}{V_M C} \times \frac{P}{P_0}, \tag{3}$$

where P and P_0 represent nitrogen saturated vapor pressure at nitrogen partial pressure and liquid nitrogen temperature, respectively. V represents the actual adsorption amount of nitrogen on the sample surface; V_M represents the saturated adsorption capacity of the nitrogen monolayer; C is a constant related to the adsorption capacity of the sample. According to IUPAC classification criteria, the N_2 adsorption-desorption isotherms of MIL-53/D201 composite are intermediate between type I and type IV in the relative pressure range, with hysteresis rings corresponding to micropores [38]. The pore size distribution curve of BJH shows that the pore sizes are concentrated at 2.9 and 141 nm, corresponding to micropores and macropores, respectively.
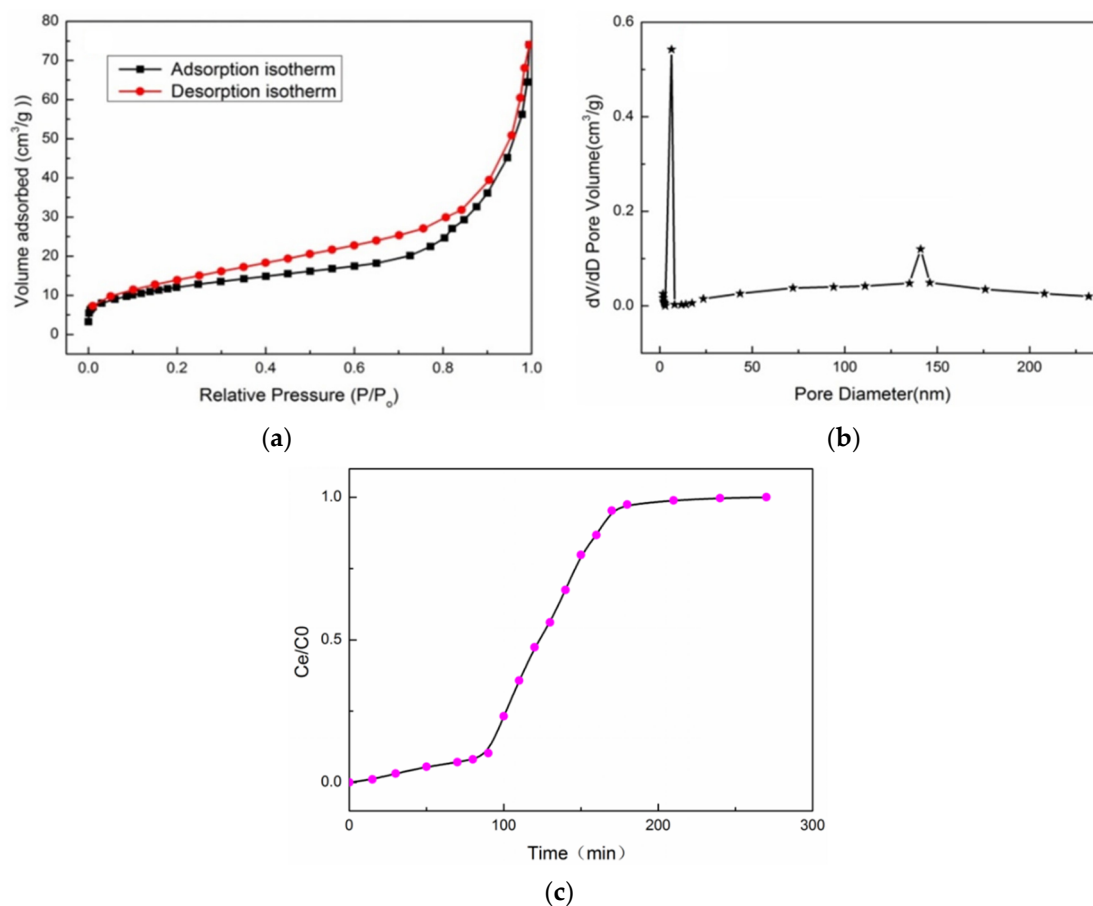
(**a**)

(**b**)

(**c**)

Figure 6. N$_2$ adsorption-desorption isotherms (**a**) and BJH pore size distributions (**b**), and penetration curve of azlocillin sodium (**c**).

3.2. Penetration Curve

One of the main parameters in the selection of adsorbents for industrial applications is the adsorption penetration time. In the whole adsorption process, when the simulated wastewater flows out of the penetrating column with adsorbent under the condition of constant liquid concentration, the corresponding point of the corresponding penetration curve when the outflow concentration Ce reaches 5% of the initial concentration C$_0$ (C$_e$/C$_0$ = 0.05) is called the penetration point [39]. When the outlet concentration of the adsorption column is equal to 95% of the initial concentration of the solution (C$_e$/C$_0$ = 0.95), the adsorption saturation is achieved. The penetration time is the time required from the beginning of adsorption to the point of penetration [40]. The time from the beginning of adsorption to the composite material to reach the adsorption saturation time is the adsorption saturation time. The penetration curve of MIL-53/D201 composite material adsorbing azlocillin sodium solution (1 mmol/L) at a constant flow rate was studied (Figure 6c). Figure 6c shows that, before 165 min, the adsorption capacity of MIL-53/D201 composite continued to increase because MIL-53/D201 composite has a large specific surface area and a large number of active adsorption sites. These active adsorption sites were occupied over time and reached equilibrium after 165 min. When MIL-53/D201 composite material adsorbed sodium azlocillin, the C$_e$/C$_0$ = 0.05 time was about 40 min (Table 1), and the adsorption saturation time was about 165 min.

Table 1. Penetration time and saturation time of azlocillin sodium.

Adsorbate (0.1 mmol/L)	Penetration Time (min)	Saturation Time (min)
Azlocillin sodium	40	165

3.3. Effect of the Adsorbent Addition Amount

Figure 7a shows the adsorption effect of MIL-53/D201 composite material on azlocillin sodium solution at different dosages (20, 40, 100, and 200 mg). With the increase in dosage, the adsorption capacity of MIL-53/D201 composite adsorbent to azlocillin sodium increased gradually, but the unit adsorption capacity showed a decreasing trend. This is because, as the dosage increases, the specific surface area and active adsorption site provided by the adsorbent increase, but the amount of adsorbate (azlocillin sodium) in the solution remains constant. It was observed that when the dosage was 20 and 40 mg, the adsorption of azlocillin sodium on the composite was basically saturated at 240 min. When the dosages were 100 and 200 mg, the adsorption of azlocillin sodium on the composites reached saturation after 120 min. The comparative experiment showed that when the dosage is 100 mg, the adsorption effect can be improved, and the adsorbent will not be wasted.
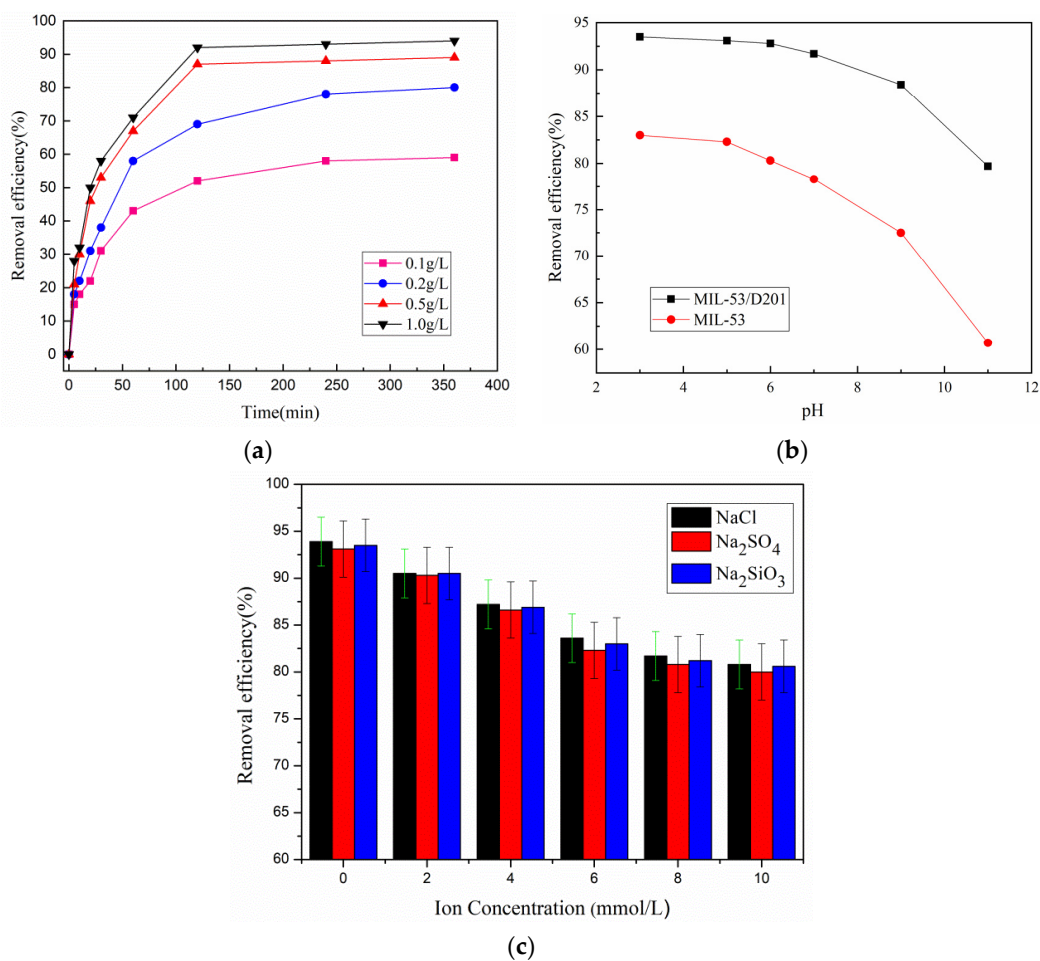

Figure 7. The effect of the addition amount of MIL-53/D201 (**a**), solution pH (**b**), and interfering ions (**c**) on the removal of azlocillin sodium.

3.4. Effect of pH of the Solution

The adsorption of the adsorbent in the pollutant solution depends largely on the pollutant solution's pH. In this experiment, the influence of the pH on the removal rate of MIL-53/D201 composite and MIL-53 was investigated. This influence determines the existence form of the target ion and the possible change in the surface charge of the adsorbent. As shown in Figure 7b, the adsorption of MIL-53/D201 composite and MIL-53 adsorbents on azlocillin sodium solution under different pH conditions was investigated. The results showed that the adsorption effects of the two adsorbents were significantly improved under weak acid conditions, and the maximum removal rates were 93.9% and

83.3%, respectively. For MIL-53, this is because a lower pH value facilitates the release of a higher concentration of H^+, and MIL-53 has a positive potential. Azlocillin sodium in aqueous solution is an anionic ligand with the ability to give a pair of electrons (Lewis base), and has a strong electrostatic interaction with the central Fe^{3+} (Lewis acid) in the MIL-53 framework. This explains the high adsorption capacity of MIL-53 for azlocillin sodium under acidic conditions. However, the π-π interaction between MIL-53 and the benzene ring of azlocillin sodium and the respiratory effect of MIL-53 may also be the existing mechanism [41]. For MIL-5/D201 composite, not only was the adsorption performance of MIL-53 improved, but its D201 macroporous resin was able to preconcentrate target anions through quaternary amine groups, so as to achieve more efficient adsorption. As a result of the increase in pH value, the adsorption capacity of MIL-53 decreased significantly, because the increasing OH^- in the solution can compete with the anions in azlocillin sodium, reducing the adsorption capacity of MIL-53. In addition, the number of negatively charged sites also increases. MOF materials are unstable in strong alkali conditions (especially in the case of terephthalic acid as the linker) and will gradually dissolve and reduce the adsorption performance.

It is worth noting that MIL-53/D201 composite also has a high adsorption capacity under alkaline conditions. This stability is attributed to the protection of crosslinked polystyrene matrix, so the adsorption capacity of MIL-53/D201 composite to azlocillin sodium is significantly higher than MIL-53 at the same pH value.

3.5. Effect of Interfering Ions in Solution

The adsorption process of adsorbents is affected by other ions in water. The results show that the adsorption properties of D201 resin are affected differently by different kinds and concentrations of anions. In general, a greater concentration of anions will affect the resin adsorption. This is because the anions occupy the active adsorption site on the resin, hindering the resin adsorption of the adsorbent; this phenomenon is competitive adsorption. Therefore, Cl^-, SO_4^{2-}, and SiO_3^{2-} were selected as interfering ions in this experiment to explore the adsorption effect of MIL-53/D201 composite on azlocillin sodium (Figure 7c). It can be seen from Figure 7c that the influence of these three interfering ions on the adsorption efficiency of MIL-53/D201 composite is $SO_4^{2-} > SiO_3^{2-} > Cl^-$. With the increase in the concentration of interfering ions, the removal efficiency of MIL-53/D201 composite adsorbent decreased successively. However, when the concentration of interfering ions increased to 8 mmol/L, the removal efficiency of MIL-53/D201 composite basically did not decrease any further, because the interfering ions engaged in competitive adsorption with anions in azlocillin sodium. The selective adsorption of target anions by D201 macroporous resin is hindered, and the greater the concentration of interfering ions is, the more obvious it is. Due to the presence of MIL-53 in the composite adsorbent, the adsorption of target anions can be continued through electrostatic interaction, which effectively indicates that when the concentration of interfering ions increases to a certain extent, the removal efficiency of MIL-53/D201 composite does not continue to decrease.

3.6. Adsorption Kinetics

In order to better study the adsorption process of MIL-53/D201 on azlocillin sodium, Lagergren's pseudo-first-order and pseudo-second-order dynamics were used for fitting analysis, and the simulation diagram of adsorption kinetics is shown in Figure 8a. The adsorption kinetic parameters (Table 2) were obtained from the pseudo-first-order model equation (Formula (4)) and the pseudo-second-order model equation (Formula (5)), where the first-order kinetic coefficient R^2 was 0.942.

$$Log(q_e - q_t) = Log q_e - \frac{k_1 t}{2.303}, \tag{4}$$

$$\frac{t}{q_t} = \frac{1}{k_2 q_e^2} + \frac{t}{q_e}, \tag{5}$$

where k_1 and k_2 represent the rate constant of the pseudo-first-order model ($L \cdot min^{-1}$) and pseudo-second-order model ($g \cdot mg^{-1} \cdot min^{-1}$) respectively. q_e and q_t are the adsorption capacity at equilibrium ($mg \cdot g^{-1}$) and adsorption capacity at t ($mg \cdot g^{-1}$), respectively. It can be seen from the comparison that the equilibrium adsorption amount obtained in the actual experiment is quite different from the equilibrium adsorption amount obtained by the fitting results. Therefore, the adsorption process of MIL-53/D201 composite is not suitable to be described by pseudo-first-order kinetics; that is, the adsorption of MIL-53/D201 composite is not simple physical adsorption of azlocillin sodium. It can be seen from Table 2 that the R^2 correlation coefficient of the quasi-second-order kinetic equation is 0.957, and the equilibrium adsorption amount obtained in the actual experiment is closer to that obtained through fitting results, indicating that the adsorption process is more consistent with the quasi-second-order kinetic adsorption model. This indicates that the chemisorption of MIL-53/D201 composite to azlocillin sodium is dominant. The fitting results show that the whole adsorption process of MIL-53/D201 composite followed the quasi-second-order kinetic model; that is, chemical adsorption was the main process.
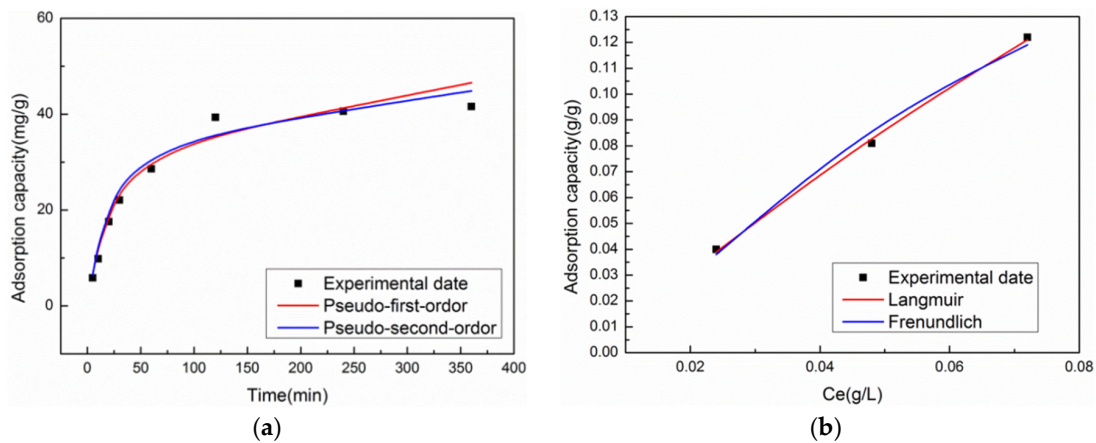

Figure 8. Kinetic fitting diagram (**a**) and thermodynamic fitting diagram (**b**) of adsorption of azlocillin sodium by MIL-53/D201 composite.

Table 2. Kinetic fitting parameters and thermodynamic fitting parameters of azlocillin sodium adsorption by MIL-53/D201 composite.

	R^2	K
Pseudo-first-order	0.942	0.254
Pseudo-second-order	0.957	0.084
Langmuir	0.993	2.056
Freundlich	0.987	0.182

3.7. Thermodynamics of Adsorption

The Langmuir isothermal adsorption model (Formula (6)) and Freundlich isothermal adsorption model (Formula (7)) were used to combine the adsorption data of MIL-53/D201 composite for azlocillin sodium solution. The thermodynamic fitting diagram is shown in Figure 8b, and the fitting parameters are shown in Table 2. The Langmuir thermodynamic fitting parameter R^2 was 0.993, which was larger than the Freundlich thermodynamic fitting parameter R^2, indicating that the adsorption process of MIL-53/D201 composite material for sodium azlocillin followed the Langmuir adsorption isothermal model; that is, monolayer adsorption was predominant. The maximum saturated adsorption capacity was 122.3 mg/g. The linearized Langmuir model is expressed by the following equation:

$$\frac{C_e}{q_e} = \frac{1}{q_m K_1} + \frac{C_e}{q_m}, \tag{6}$$

where C_e is the equilibrium concentration (mg/L). q_e and q_m represent the adsorption capacity (mg/g) and maximum adsorption capacity (mg/g) at equilibrium, respectively. K_1 is the Langmuir adsorption constant (L/mg). The parameters q_m, K_1, and correlation coefficient R^2 are determined by the linear regression between C_e/q_e and C_e. The Freundlich model can also be applied to non-ideal systems, including multilayer adsorption on heterogeneous media surfaces, expressed by the following equation:

$$q_e = K_F C_e^{\frac{1}{n}}, \tag{7}$$

where C_e and q_e represent equilibrium concentration (mg/L) and adsorption capacity (mg/g), respectively. K_F and n represent the Freundlich constant. The parameters K_F, $1/n$, and correlation coefficient R^2 are determined by the linear regression relationship between q_e and $\log C_e$ [42]. An n value between 1 and 10 indicates that adsorption is favorable. A low n value indicates that there are bad adsorption conditions and competitive adsorption may exist.

3.8. Adsorption Regeneration

In practical applications, the reusability of adsorbents is a very important parameter in terms of cost effectiveness. Compared with powdered MOF, MOF/D201 composite adsorbent not only has higher adsorption performance, but also can achieve adsorption regeneration through simple ethanol immersion. The used ethanol can still be used for the next cycle, effectively avoiding waste. In this study, ethanol was used as a desorption agent for MIL-53/D201 composite after adsorption. After five sorption-desorption cycles, the results obtained are shown in Figure 9a. After four cycles, the removal efficiency tended to be stable, and was still about 83%. These results indicate that MIL-53/D201 adsorbent has good reusability and can be used in water treatment for a long period.
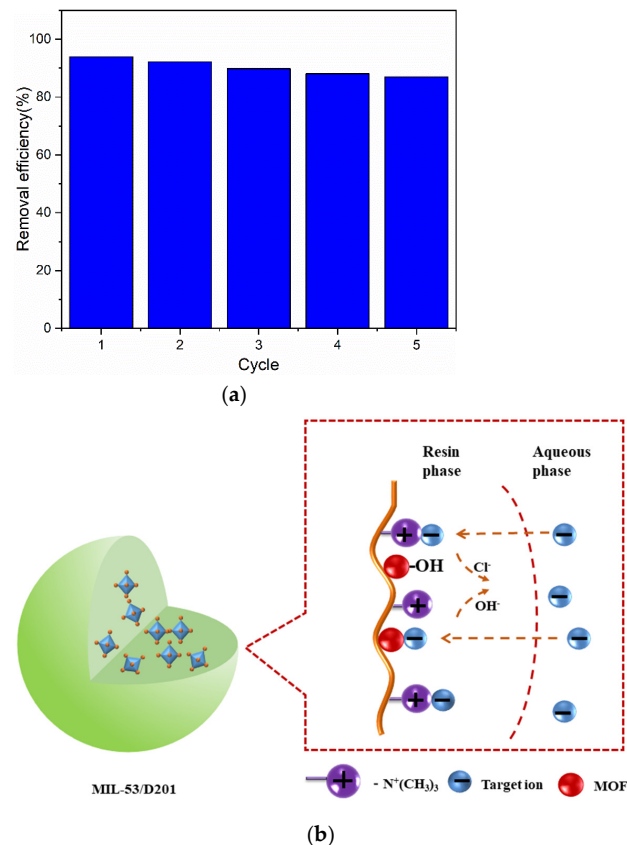
(a)

(b)

Figure 9. Adsorption regeneration diagram (**a**) and adsorption mechanism diagram (**b**) of removing azlocillin sodium by MIL-53/D201.

4. Conclusions

In this paper, MIL-53 was in situ synthesized in D201 anion exchange resin by the hydrothermal synthesis method. A new MIL-53/D201 composite was prepared and the adsorption effect of the composite on azlocillin sodium in solution was studied. The structural characteristics, functional groups, and thermal analysis of MIL-53 and MIL-53/D201 composite were studied by XRD, SEM, EDS, and BET. The results showed that D201 as the carrier not only did not destroy the original structure of MOF material, but also caused the composite material to have a larger specific surface area and more stable and efficient adsorption performance.

Through the adsorption exploration experiment, it was found that the composite material can overcome the disadvantages of MOF material instability in the water phase and easy dissociation in strongly alkaline conditions. The composite was also shown to have the characteristics of stable and efficient adsorption. The adsorption mechanism can be explained by electrostatic interaction between -NR$_3^+$ in D201 resin and anions in pollutants, the π-π interaction between the MIL-53 aromatic ring and azlocillin sodium, and the coordination of MIL-53 and hydrogen bonding (Figure 9). The adsorption process was more consistent with the quasi-second-order kinetic adsorption model and Langmuir isothermal adsorption model; that is, chemical adsorption and monolayer adsorption were the main adsorption processes, and the maximum saturated adsorption capacity was 122.3 mg/g. In conclusion, this study provides an idea for the fixation of MOF materials in stable carriers, and this novel composite adsorbent material can be used as a potential material for the degradation of target anionic pollutants in water.

References

1. Xie, H.; Du, J.; Chen, J. Concerted Efforts Are Needed to Control and Mitigate Antibiotic Pollution in Coastal Waters of China. *Antibiotics* **2020**, *9*, 88. [CrossRef]
2. Li, J.; Wang, X.; Zhao, G.; Chen, C.; Chai, Z.; Alsaedi, A.; Hayat, T.; Wang, X. Metal-organic framework-based materials: Superior adsorbents for the capture of toxic and radioactive metal ions. *Chem. Soc. Rev.* **2018**, *47*, 2322–2356. [CrossRef] [PubMed]
3. Bobbitt, N.S.; Mendonca, M.L.; Howarth, A.J.; Islamoglu, T.; Hupp, J.T.; Farha, O.K.; Snurr, R.Q. Metal-organic frameworks for the removal of toxic industrial chemicals and chemical warfare agents. *Chem. Soc. Rev.* **2017**, *46*, 3357–3385. [CrossRef] [PubMed]
4. Mon, M.; Bruno, R.; Ferrando-Soria, J.; Armentano, D.; Pardo, E. Metal-organic framework technologies for water remediation: Towards a sustainable ecosystem. *J. Mater. Chem. A* **2018**, *6*, 4912–4947. [CrossRef]
5. Hasan, Z.; Jhung, S.H. Removal of hazardous organics from water using metal-organic frameworks (MOFs): Plausible mechanisms for selective adsorptions. *J. Hazard. Mater.* **2015**, *283*, 329–339. [CrossRef] [PubMed]
6. Martínez, J.L. Antibiotics and antibiotic resistance genes in natural environments. *Science* **2008**, *321*, 365–367. [CrossRef] [PubMed]
7. Gaikwad, S.; Cheedarala, R.K.; Gaikwad, R.; Kim, S.; Han, S. Controllable Synthesis of 1,3,5-tris (1H-benzo [d] imidazole-2-yl) Benzene-Based MOFs. *J. Appl. Sci.* **2021**, *11*, 9856. [CrossRef]

8. Howarth, A.J.; Liu, Y.; Hupp, J.T.; Farha, O.K. Metal-organic frameworks for applications in remediation of oxyanion/cation-contaminated water. *CrystEngComm* **2015**, *17*, 7245–7253. [CrossRef]

9. Zou, Y.; Wang, X.; Khan, A.; Wang, P.; Liu, Y.; Alsaedi, A.; Hayat, T.; Wang, X. Environmental remediation and application of nanoscale zero-valent iron and its composites for the removal of heavy metal ions: A review. *Environ. Sci. Technol.* **2016**, *50*, 7290–7304. [CrossRef]

10. Wu, X.; Tan, X.; Yang, S.; Wang, P.; Liu, Y.; Alsaedi, A.; Hayat, T.; Wang, X. Coexistence of adsorption and coagulation processes of both arsenate and NOM from contaminated groundwater by nanocrystallined Mg/Al layered double hydroxides. *Water Res.* **2013**, *47*, 4159–4168. [CrossRef] [PubMed]

11. Hadi, P.; To, M.H.; Hui, C.W.; Lin, C.S.K.; McKay, G. Aqueous mercury adsorption by activated carbons. *Water Res.* **2015**, *73*, 37–55. [CrossRef]

12. Hoskins, B.F.; Robson, R. Infinite polymeric frameworks consisting of three dimensionally linked rod-like segments. *J. Am. Chem. Soc.* **1989**, *111*, 5962–5964. [CrossRef]

13. Colinas, I.R.; Silva, R.C.; Oliver, S.R.J. Reversible, selective trapping of perchlorate from water in record capacity by a cationic metal-organic framework. *Environ. Sci. Technol.* **2016**, *50*, 1949–1954. [CrossRef]

14. Zhu, L.; Xiao, C.; Dai, X.; Li, J.; Gui, D.; Sheng, D.; Chen, L.; Zhou, R.; Chai, Z.; Albrecht-Schmitt, T.E.; et al. Exceptional perrhenate/pertechnetate uptake and subsequent immobilization by a low-dimensional cationic coordination polymer: Overcoming the hofmeister bias selectivity. *Environ. Sci. Technol. Lett.* **2017**, *4*, 316–322. [CrossRef]

15. Bhadra, B.N.; Seo, P.W.; Khan, N.A.; Jhung, S.H. Hydrophobic cobalt-ethylimidazolate frameworks: Phase-pure syntheses and possible application in cleaning of contaminated water. *Inorg. Chem.* **2016**, *55*, 11362–11371. [CrossRef] [PubMed]

16. Farha, O.K.; Eryazici, I.; Jeong, N.C.; Hauser, B.G.; Wilmer, C.E.; Sarjeant, A.A.; Snurr, R.Q.; Nguyen, S.T.; Yazaydin, A.O.; Hupp, J.T. Metal-organic framework materials with ultrahigh surface areas: Is the sky the limit? *J. Am. Chem. Soc.* **2012**, *134*, 15016–15021. [CrossRef]

17. Alaerts, L.; Maes, M.; Giebeler, L.; Jacobs, P.A.; Martens, J.A.; Denayer, J.F.; Kirschhock, C.E.; De Vos, D.E. Selective Adsorption and Separation of Ortho-Substituted Alkylaromatics with the Microporous Aluminum Terephthalate MIL-53. *J. Am. Chem. Soc.* **2008**, *130*, 14170–14178. [CrossRef] [PubMed]

18. Gwon, K.; Han, I.; Lee, S.; Kim, Y.; Lee, D.N. Novel metal–organic framework-based photocrosslinked hydrogel system for efficient antibacterial applications. *ACS Appl. Mater. Interfaces* **2020**, *12*, 20234–20242. [CrossRef]

19. Gwon, K.; Kim, Y.; Cho, H.; Lee, S.; Yang, S.H.; Kim, S.J.; Lee, D.N. Robust Copper Metal–Organic Framework-Embedded Polysiloxanes for Biomedical Applications: Its Antibacterial Effects on MRSA and In Vitro Cytotoxicity. *Nanomaterials* **2021**, *11*, 719. [CrossRef] [PubMed]

20. Ma, X.; Wang, W.; Sun, C.; Li, H.; Sun, J.; Liu, X. Adsorption performance and kinetic study of hierarchical porous Fe-based MOFs for toluene removal. *Sci. Total Environ.* **2021**, *793*, 148622. [CrossRef] [PubMed]

21. Shen, K.; Zhang, L.; Chen, X.; Liu, L.; Zhang, D.; Han, Y.; Chen, J.; Long, J.; Luque, R.; Li, Y.; et al. Ordered macro-microporous metal-organic framework single crystals. *Science* **2018**, *359*, 206–210. [CrossRef]

22. Ou, R.; Zhang, H.; Wei, J.; Kim, S.; Wan, L.; Nguyen, N.S.; Hu, Y.; Zhang, X.; Simon, G.P.; Wang, H. Thermoresponsive amphoteric metal-organic frameworks for efficient and reversible adsorption of multiple salts from water. *Adv. Mater.* **2018**, *30*, 1802767. [CrossRef] [PubMed]

23. Valizadeh, B.; Nguyen, T.N.; Smit, B.; Stylianou, K.C. Porous Metal-Organic Framework@ Polymer Beads for Iodine Capture and Recovery Using a Gas-Sparged Column. *Adv. Funct. Mater.* **2018**, *28*, 1801596. [CrossRef]

24. McHugh, L.N.; McPherson, M.J.; McCormick, L.J.; Morris, S.A.; Wheatley, P.S.; Teat, S.J.; McKay, D.; Dawson, D.M.; Sansome, C.E.F.; Ashbrook, S.E.; et al. Hydrolytic stability in hemilabile metal-organic frameworks. *Nat. Chem.* **2018**, *10*, 1096–1102. [CrossRef]

25. Hynek, J.; Brázda, P.; Rohlíček, J.; Londesborough, M.G.; Demel, J. Phosphinic acid based linkers: Building blocks in metal-organic framework chemistry. *Angew. Chem. Int. Ed.* **2018**, *57*, 5016–5019. [CrossRef]

26. Yuan, S.; Feng, L.; Wang, K.; Pang, J.; Bosch, M.; Lollar, C.; Sun, Y.; Qin, J.; Yang, X.; Zhang, P.; et al. Stable metal-organic frameworks: Design, synthesis, and applications. *Adv. Mater.* **2018**, *30*, 1704303. [CrossRef]

27. Liang, R.; Jing, F.; Shen, L.; Qin, N.; Wu, L. MIL-53(Fe) as a highly efficient bifunctional photocatalyst for the simultaneous reduction of Cr(VI) and oxidation of dyes. *J. Hazard. Mater.* **2015**, *287*, 364–372. [CrossRef]

28. Du, J.; Yuan, Y.; Su, J.; Peng, F.; Jiang, X.; Qiu, L.; Xie, A.; Shen, Y.; Zhu, J. New photocatalysts based on MIL-53 metal-organic frameworks for the decolorization of methylene blue dye. *J. Hazard. Mater.* **2011**, *190*, 945–951. [CrossRef] [PubMed]

29. Zhu, B.J.; Yu, X.Y.; Jia, Y.; Peng, F.M.; Sun, B.; Zhang, M.Y.; Lou, T.; Liu, J.H.; Huang, X.J. Iron and 1, 3, 5-benzenetricarboxylic metal-organic coordination polymers prepared by solvothermal method and their application in efficient As (V) removal from aqueous solutions. *J. Phys. Chem. C* **2012**, *116*, 8601–8607. [CrossRef]

30. Molinari, A.; Varani, G.; Polo, E.; Vaccari, S.; Maldotti, A. Photocatalytic and catalytic activity of heterogenized W10O324—In the bromide-assisted bromination of arenes and alkenes in the presence of oxygen. *Mol. Catal. A Chem.* **2007**, *262*, 156–163. [CrossRef]

31. Zhang, X.; Cheng, C.; Qian, J.; Lu, Z.; Pan, S.; Pan, B. Highly efficient water decontamination by using sub-10 nm FeOOH confined within millimeter-sized mesoporous polystyrene beads. *Environ. Sci. Technol.* **2017**, *51*, 9210–9218. [CrossRef]

32. Zhang, X.; Wu, M.; Dong, H.; Li, H.; Pan, B. Simultaneous oxidation and sequestration of As (III) from water by using redox polymer-based Fe (III) oxide nanocomposite. *Environ. Sci. Technol.* **2017**, *51*, 6326–6334. [CrossRef] [PubMed]

33. Liu, F.; Shan, C.; Zhang, X.; Zhang, Y.; Zhang, W.; Pan, B. Enhanced removal of EDTA-chelated Cu (II) by polymeric anion-exchanger supported nanoscale zero-valent iron. *J. Hazard. Mater.* **2017**, *321*, 290–298. [CrossRef]

34. Araya, T.; Jia, M.; Yang, J.; Zhao, P.; Cai, K.; Ma, W.; Huang, Y. Resin modified MIL-53 (Fe) MOF for improvement of photocatalytic performance. *J. Appl. Catal. B Environ.* **2017**, *203*, 768–777. [CrossRef]

35. Ai, L.; Zhang, C.; Li, L.; Jiang, J. Iron terephthalate metal-organic framework: Revealing the effective activation of hydrogen peroxide for the degradation of organic dye under visible light irradiation. *Appl. Catal. B Environ.* **2014**, *148*, 191–200. [CrossRef]

36. Gao, Y.; Li, S.; Li, Y.; Yao, L.; Zhang, H. Accelerated photocatalytic degradation of organic pollutant over metal-organic framework MIL-53 (Fe) under visible LED light mediated by persulfate. *Appl. Catal. B Environ.* **2017**, *202*, 165–174. [CrossRef]

37. Huang, W.; Liu, N.; Zhang, X.; Wu, M.; Tang, L. Metal organic framework g-C_3N_4/MIL-53 (Fe) heterojunctions with enhanced photocatalytic activity for Cr (VI) reduction under visible light. *Appl. Surf. Sci.* **2017**, *425*, 107–116. [CrossRef]

38. Zhang, N.; Yuan, L.Y.; Guo, W.L.; Luo, S.Z.; Chai, Z.F.; Shi, W.Q. Extending the use of highly porous and functionalized MOFs to Th (IV) capture. *ACS Appl. Mater. Interfaces* **2017**, *9*, 25216–25224. [CrossRef]

39. Yao, M.; Dong, Y.; Feng, X.; Hu, X.; Jia, A.; Xie, G.; Hu, G.; Lu, J.; Luo, M.; Fan, M. The effect of post-processing conditions on aminosilane functionalizaiton of mesocellular silica foam for post-combustion CO_2 capture. *Fuel* **2014**, *123*, 66–72. [CrossRef]

40. Wan, D.; Ma, X.; Sentorun-Shalaby, C.; Song, C. Development of carbon-based "molecular basket" sorbent for CO_2 capture. *Ind. Eng. Chem. Res.* **2012**, *51*, 3048–3057.

41. Haque, E.; Jun, J.W.; Jhung, S.H. Adsorptive removal of methyl orange and methylene blue from aqueous solution with a metal-organic framework material, iron terephthalate (MOF-235). *J. Hazard. Mater.* **2011**, *185*, 507–551. [CrossRef]

42. Bandura, L.; Kołodyńska, D.; Franus, W. Adsorption of BTX from aqueous solutions by Na-P1 zeolite obtained from fly ash. *Process Saf. Environ. Prot.* **2017**, *109*, 214–223. [CrossRef]